SUPPLEMENTARY INFORMATION

IRE1 endoribonuclease signaling promotes myeloid cell infiltration in glioblastoma.

Joanna Obacz et al.

TABLE OF CONTENTS

SUPPLEMENTAL METHODS AND MATERIALS

Plasmids and siRNAs – pCMV3-UBE2D3-Flag expression plasmid was purchased from Sino Biological (Interchim), pRS shRN mouse ube2d3 (shRNA sequence: 5'-GACAGAGATAAGTACAACAGAATATCTCG-3') from Origene and pCMV5-Flag-XBP1s from Addgene. Small interfering RNA targeting the expression of MIB1 and UBE2D3 were purchased from Thermo Fisher Scientific; and of IRE1, XBP1, SYVN1 (Smartpool Dharmacon, Horizon Discovery). siRNA negative controls were purchased from Thermo Fisher Scientific and Dharmacon.

Patient samples and data – The GBMmark cohort was generated as previously described (Lhomond et al., 2018). Briefly, tumors were obtained by processing the biological samples through the Centre de Ressources Biologiques (CRB) Santé of Rennes BB-0033-00056. The research protocol was conducted under the French legal guidelines and fulfilled the requirements of the local institutional ethics committee. The quantification procedure for mRNA abundance is described in the "Microarray data analysis" section. Messenger RNA expression datasets were also assessed from the publicly available GB dataset from The Cancer Genome Atlas (TCGA) on the NCBI website platform https://gdc-portal.nci.nih.gov/ and from the TCGA-GBLGG dataset obtained from the GlioVis online tool (http://gliovis.bioinfo.cnio.es/).

Microarray data analysis – Complete gene expression analysis of the GB TCGA and GBMmark microarray Agilent dataset (GEO) was performed with R (R version 3.5.0) / Bioconductor software. Firstly, the raw data obtained from the public repository ArrayExpress (E-MTAB-6326) were pre-processed (background correction and quantile normalization) using the limma R package. Next, non-expressed probe sets in the majority of the samples (that is, probesets expressed in less than 10% of the total number of patients) were filtered out, in order to remove consistently non-expressed genes. To shed light on the molecular mechanisms involved in the IRE1-UBE2D3 signaling axis, the aforementioned list of DE genes, was used as an input to the BioInfoMiner interpretation web platform, which performs automated, network analysis of functional terms, integrating semantic information from different biomedical ontologies and controlled vocabularies such as Gene Ontology (GO), Reactome, Human Phenotype Ontology (HPO) and many others. For the transcriptome analysis for immune infiltration, hierarchical clustering of GB patients (TCGA GB cohort) labeled for their IRE1 activity (high or low), based on their ranked IRE1sign38 score obtained from (Lhomond *et al.* 2018), was coupled with the gene expression profile of immune cell markers for microglia/macrophage (MM), monocytes derived macrophages (MDM), microglia cells (MG), polynuclear neutrophils (PMN) and T cells (T) derived from the literature (Yin W et al. *J Pathol*. 2022; Bowman RL et al. *Cell Rep*. 2016; Cui X et al. *Front Oncol*. 2021). Samples

were clustered using Euclidean distance similarity metric with complete linkage. The Roast method, a parametric multivariate rotation gene set test, was used for the self-contained gene set analysis of immune cell signatures (MM, MDM, MG, PMN, and T) between IRE1_high and IRE1_low TCGA-GB tumors. For this reason, the roast () function of the limma R package was used. The “UP” and “p” values denote the “PropUp” and “PValue” output components of roast, that is the proportion of signature genes that were found up-regulated between the groups under study and the estimated two-sided directional p-value of test, respectively. n denotes the number of signature genes. MM markers (41 genes): ACHE, AIF1, APOL3, ARRB1, BHLHE41, CCL2, CCL7, CCL14, CCL23, CD14, CD36, CD40, CD68, CD80, CD86, CD163, COL8A2, CRYBB1, CSF1, CXCL5, CXCL9, CYP27B1, DCSTAMP, FCGR1A, FCGR1B, FRMD4A, GPC4, HLA-DRA, HLA-DRB1, HRH1, IL6, KIAA0754, MARCO, MMP9, MRC1, NPL, PPBP, RENBP, SLAMF1, TRPM4, WNT5B. MDM markers (35 genes): ASPM, CCL20, CCR1, CD163, CD68, CDCA3, CIITA, CXCL2, CXCL3, CXCL5, IL8, CXCR4, ENO1, FAS, HLA-DMB, HGF, HLA-DQA1/2, IFITM1, IFITM2, IL1B, IL1R2, IL1RN, IL7R, ITGA4, KMO, KYNU, LGALS3, LYZ, PLIN2, S100A11, S100A9, THBD, THBS1, TIMP1, TNFSF13. MG markers (27 genes): ATF3, C2, C4b, CCL3, CCL4, CFH, CH25H, CYTL1, DHCR24, EGR3, ETV5, FGF13, FOS, FOSB, IFI27, IFIT3, JAM2, LOX, MEF2C, MMP9, OLFML3, SALL1, SGK1, SLC2A5, TGFA. PMN markers (25 genes): ANPEP, ARG1, BTNL8, CASP5, CCR3, CD177, CEACAM3, CXCR1, CXCR2, ELANE, FCGR3B, FPR2, FUT4, HAL, HSPA6, ITGAX, LAMP3, MMP25, MPO, PGLYRP1, STEAP4, THBD, TNFRSF10C, TREM1, VNN3. T markers (35 genes): ACAP1, ANKRD55, CD8A, CD8B, CDC25A, CRTAM, DUSP2, EPB41, EPHA1, ETS1, FBXL8, GAL3ST4, GALR1, GNLY, KLF3-AS1, KLRC3, KLRC4, KLRD1, KLRF1, KLRK1, MAP4K2, NCR3, NKG7, ORC1, PBXIP1, PIK3IP1, RASGRP2, RPL10L, RRP9, SERGEF, SKA1, VILL, WNT7A, ZFP36L2, ZNF324. Barcode plot visualization of the results of the self-contained ROAST gene set test for the immune cell signatures (PMN, MM and T) of TCGA-GB tumors. Barcode plots were made using the barcodeplot() function of the limma R package. Differentially expressed genes from IRE1_high vs IRE1_low TCGA-GB-RNAseq tumors, were ranked from left to right by increasing log-fold-change in the background of the barcode plot. Blue bar on the left defines the direction of the down-regulated genes in IRE1_high GB tumors and the red bar on the right defines the direction of up-regulated genes. The curve (or worm) above the barcode shows the enrichment of the vertical black bars (signature genes) amongst low or high ranked genes of TCGA-GB-RNAseq tumors. The dotted horizontal line indicates neutral enrichment; the worm above the dotted line shows enrichment while the worm below the dotted line shows depletion. X-axis shows logFC for IRE1_high vs IRE1_low TCGA-GB-RNAseq tumors. Black bars represent signature genes. The curve (or worm) shows relative enrichment.

Cell culture and treatments – For certain tumors, the two types of cultures have been established, adherent cell lines (RADH) grown in DMEM supplemented with 10% FCS and neurospheres (RNS, enriched in cancer stem cells) grown in DMEM/Ham's F12 GlutaMAX (Life Technologies) supplemented with B27 and N2 additives (Invitrogen), EGF (20 ng/ml) and FGF2 (20 ng/ml) (Peprotech, Tebu-Bio) as described previously (Avril *et al.*, 2012). The analysis of genetic background i.e. copy number variants and alterations using CNVkit, BreakDancer and DELLY tools revealed that the RADH87 cell line carried features previously described in GB including EGFR amplification, IDH1 wildtype, methylated promoter of MGMT and genetic alterations in chromosome 7 (loss and gain) and 10 (loss). For transient overexpression or silencing, cells were transfected using Lipofectamine 2000 or Lipofectamine LTX (ThermoFisher Scientific) for plasmids and Lipofectamine RNAiMAX Transfection Reagent (ThermoFisher Scientific) for siRNA, according to the manufacturer's instructions. For immune infiltration analysis, GB specimens were dissociated using the gentle MACS dissociator (Miltenyi Biotec) according to the manufacturer's recommendations and cells were directly used for flow cytometry analysis. To induce ER stress, cells were treated with 5 µg/mL tunicamycin (Tm) (Calbiochem) or 50 nM of thapsigargin (Tg) for the indicated time periods. For NFκB pathway inhibition, 5µM JSH-23 (Sigma Aldrich) was used for 16 hours.

Generation of stable cell lines – RADH87 and GL261 cells stably overexpressing UBE2D3 (hereafter referred to as RADH87_UBE2D3 and GL261_UBE2D3) were selected using 300µg/mL and 500µg/mL hygromycin B, respectively (ThermoFisher Scientific). Monoclonal cell populations were obtained using a limited dilution protocol after 10 days of antibiotic selection. Single cell clones were expanded and UBE2D3 expression was analyzed by western blotting using anti-UBE2D3 (Abcam) or anti-FLAG (Sigma Aldrich) antibodies. For stable down-expression of ube2d3, GL261 cells was transfected with 1µg of pRS shRN mouse ube2d3 (shRNA sequence: 5' GACAGAGATAAGTACAACAGAATATCTCG 3') expression plasmid using Lipofectamine 2000 (ThermoFisher Scientific), following the manufacturer's protocol. GL261 cells stably down-regulating ube2d3 were selected using 0.5 µg/mL puromycin.

Cell preparation – PBMC were isolated from the peripheral blood of healthy donors using lymphocyte separation medium (Lonza) according to the manufacturer's recommendations. PMN were isolated from the peripheral blood of healthy donors using a MACSXPRESS Neutrophil Isolation Kit (Miltenyi Biotec), according to the manufacturer's protocol. PBMC were used as the source of Mo.

Flow cytometry analyses – The population of interest was gated on the basis of the FSC/SSC criteria. The dead cell population was excluded by 7AAD staining (BD Biosciences). Data were analyzed using the FACSDiva software (BD Biosciences). GB specimens with more

than 2% stained cells of the total viable cells were considered positive for the immune marker of interest. The gating strategy for characterizing immune population has been previously described (Hussain, et al., 2006; Parney et al., 2009).

Myeloid chemoattraction assay – Migrated myeloid cells (under the Boyden chambers) were collected, washed in PBS and analyzed by flow cytometry using a Novocyte flow cytometer (Acea Biosciences). The population of interest was gated on the basis of the FSC/SSC criteria. The relative number of migrated cells was estimated using flow cytometry by counting the number of cells per microliter. For CXCR2 inhibition with the antagonist SB225002, the drug was added and maintained during the migration assay. For attraction experiences with exogenous cytokines, recombinant IL6 and IL8 (5 ng/mL) (from Peprotech) were added to the supernatants used in the Boyden chamber assays. For attraction experiences with blocking antibodies, anti-IL6 and IL8 antibodies (20 µg/mL) (from InvivoGen and Invitrogen respectively) were added to the supernatants used in the Boyden chamber assays.

Gel shift assay – DNA-binding reactions were conducted in a 20 µl mixture containing 3 µL of nuclear extracts from U87 and GL261 cells (extracted using NE-PER Nuclear and Cytoplasmic Extraction Reagents, Thermo Scientific), 1 µg of poly (dI-dC), and 4 pmol of the biotin-labeled probe at room temperature for 30 min. For the competition assay, unlabelled probes (200 ×, 20 × and 10 ×) were added to the binding reaction. Reaction products were then separated using electrophoresis. The protein-DNA complexes were transferred onto a positively charged nylon membrane (Thermo Scientific) and detected by chemiluminescence.

Immunohistochemistry – Tumor tissues were fixed in 10% neutral buffered formalin, embedded in paraffin, cut into 4-µm thick sections, mounted on slides, deparaffinized in xylene and rehydrated in PBS through a graded ethanol series. Endogenous peroxidase activity was quenched with 3% hydrogen peroxide (Roche) in PBS for 15 minutes. IHC labeling was performed using the H2P2 imaging platform of the University of Rennes.

Mass spectrometry – RADH87 parental and RADH87_UBE2D3 cells were lysed with lysis buffer composed of 20 mM Tris pH 8, 1.5 mM EDTA, 150 mM NaCl, 1% Triton X-100, 0.1% SDS, 15µM MG132, 10mM NEM (N-ethylmaleimide), 10µM deubiquitinating enzymes inhibitors (DUBi, PR-619), supplemented with proteases and phosphatases inhibitor cocktails (Roche). Total proteins were precipitated overnight with 80% ice-cold acetone. Protein pellets were then washed 3 times with 80% acetone, followed by centrifugation at 500 g for 30 mins at 4°C. Samples were alkylated and digested with trypsin at 37°C overnight and ubiquitinated peptides were enriched with PTMScan Ubiquitin Remnant Motif (K-ε-GG) Kit (Cell Signaling Technology). After Sep Pak desalting, peptides were analyzed using an Ultimate 3000 nano-

RSLC (Thermo Fisher Scientific) coupled in line with an Orbitrap ELITE (Thermo Scientific). Each sample was analyzed in triplicate. Briefly, peptides were separated on a C18 nano-column with a linear gradient of acetonitrile and analyzed in a Top 20 CID (Collision-induced dissociation) data-dependent mass spectrometry. Data were processed by database searching against Human Uniprot Proteome database using Proteome Discoverer 2.2 software (Thermo Fisher Scientific). Precursor and fragment mass tolerance were set at 7 ppm and 0.6 Da respectively. Trypsin was set as enzyme, and up to 2 missed cleavages were allowed. Oxidation (M, +15.995), GG (K, +114.043) were set as variable modification and Carbamidomethylation (C) as fixed modification. Proteins were filtered with False Discovery Rate <1% (high confidence). Lastly, quantitative values were obtained from Extracted Ion Chromatogram (XIC) and p-values were determined by ANOVA with Precursor Ions Quantifier node in Proteome Discoverer.

Cell proliferation – GL261 cells parental, overexpressing or silenced for UBE2D3 were cultured in 96-well plates at the concentration of $1x10^3$ cells/well and the growth rate was measured daily for 7 days. Twenty microliters of the WST1 reagent (Roche) was added to the cells, followed by 4 hours incubation at 37°C and optic densities (OD) measurements with Tecan Infinite® 200 Pro spectrophotometry (Thermo Fisher Scientific) at 450 nm and 595 nm. Specific OD was obtained by calculating the difference between the OD at 450 nm and that at 595 nm and compared to the specific OD determined for DMEM alone.

Chemokines secretion analysis – To evaluate the concentration of chemokines in tumor conditioned media, a Bio-Plex Multiplex immunoassays (Bio-Rad) was used following manufacturer protocol.

Syngeneic mouse model and inflammation – Eight-weeks old male C57BL/6 mice were housed in an animal care unit authorized by the French Ministries of Agriculture and Research (Biosit, Rennes, France - Agreement No. C35-238-40/No DIR 13480) and approved by the local (University of Rennes) ethics committee and ensuring the breeding and the daily monitoring of the animals in the best conditions of wellbeing according to the law and the rule of 3R (Reduce-Refine-Replace). The protocol used was as previously described (Le Reste *et al.* 2020). Cell implantations (50 000 cells in 1 µL) were at 2 mm lateral to the bregma and 3 mm in depth using GL261 (control), GL261_UBE2D3 or CT2A cells. For treatment with the IRE1 inhibitor B2-1 (Chevet *et al.*, 2023), mice were treated with 0.3 mg/kg of B2-1 (intra-peritoneal injection) 4 days after the tumor injection, 5 days a week during 3 weeks. Mice were daily clinically monitored and sacrificed twenty-four days post injection. Mouse brains were collected, fixed in 4% formaldehyde solution and paraffin embedded for histological analysis using anti-vimentin antibody (Interchim) to visualize the tumor masses. Tumor volume was then estimated by measuring the length (L) and width (W) of each tumor and was calculated

using the following formula ($L \times W^2 \times 0.5$). Immune cells infiltration was monitored by immunohistochemistry using rat anti-mouse Ly6G antibody (BD Biosciences) for neutrophils, anti-IBA1 (Wako) for macrophages/microglia, while NFκB level was determined with rabbit monoclonal anti-NFκB p65 antibody (Cell Signaling). Imaging was carried out using a Axioplan 2 epifluorescent microscope (Zeiss) equipped with a digital camera Axiocam (Zeiss).

Statistical analyses – Graphs and statistical analyses were performed using GraphPad Prism 7.0 software (GraphPad Software). Data are presented as the mean ± SD or SEM of at least three biological replicates. Statistical significance was determined using a paired or unpaired t-test or ANOVA as appropriate, while comparison of survival curves was performed using the log-rank (Mantel-Cox) test. Significant variations are represented by asterisks above the corresponding bar when comparing test and control conditions, and above the line when comparing the two indicated conditions.

SUPPLEMENTAL RESULTS

To identify the putative E3 ligase(s) involved in IκB degradation and/or NFκB activation as well as to investigate the global effect of UBE2D3 on protein ubiquitination in GB, we carried out a label-free quantitative MS/MS analysis using cells stably overexpressing UBE2D3 (**Fig.S5**). Total proteins were extracted from RADH87 control and RADH87_UBE2D3 cells treated with or without the ER stress inducer tunicamycin and precipitated. They were then subjected to trypsin digestion, followed or not by purification of ubiquitin-derived diglycine (di-Gly) remnants and concomitant MS/MS analysis of both ubiquitinated and total peptides (**Fig.S5A**). Among the significantly up- and down-regulated proteins in UBE2D3 overexpressing cells compared control, we identified a set of proteins involved in proteostasis control as well as in inflammatory response (**Fig.S5B**). Furthermore, we found a tight interaction between those ER-related entities that mainly function in protein metabolic processes (**Fig.S5C**) and showed an enriched association with extracellular vesicles (**Fig.S5D**), thereby highlighting a key role of UBE2D3 in the ER protein turnover and secretion. We next compared the differentially ubiquitinated proteins between the most extreme conditions, namely RADH87 control (EV) cells cultivated without stress and RADH87_UBE2D3 cells treated with tunicamycin, which would include the UBE2D3 effect on protein ubiquitination in both basal and ER stress conditions (**Fig.S5E**). We identified forty-five proteins, whose ubiquitination was significantly altered in the context of UBE2D3 overexpression and ER stress (**Fig.S5F**). Interestingly, when intersecting lists of those significantly up- and downregulated ubiquitinated proteins, we found that only one was shared between groups (**Fig.S5G**), suggesting that UBE2D3 engaged distinct machineries to exert its E2 functions in basal ER physiology or response to ER stress. Functional enrichment analysis further revealed that UBE2D3 mainly mediates ubiquitination of proteins involved in cellular response to environmental stresses, while it abrogated the ubiquitin/proteasome system-dependent degradation of proteins associated with ER-to-Golgi transport (**Fig.S5H**), which further supports our findings on UBE2D3 role in ER homeostasis regulation and secretory pathway.

SUPPLEMENTAL INFORMATION

Acknowledgements

We thank John Patterson and Qinping Zheng from Orinove Inc. (Newbury Park, USA) and Fosun Orinove PharmaTech Inc. (Jiangsu, China) respectively for providing the IRE1 inhibitor MKC8866. We thank the Biosit histopathology H2P2 platform (Université de Rennes, France) and Florence Jouan for immunohistochemical analyses of tumor xenografts; and the Biosit ARCHE animal facility (Université de Rennes) for animal housing.

Fellowships

JO was supported by a post-doctoral fellowship from Région Bretagne. KB was supported by a doctoral fellowship from INSERM and Région Bretagne. DS was supported by an AIRC fellowship for Abroad. EMG was supported by a post-doctoral fellowship from the Institut des Neurosciences Cliniques de Rennes. EL was supported by post-doctoral fellowships from the Fondation ARC and Fondation de France.

Author Contributions

JO – conceptualization, methodology, investigation, formal analysis, writing (original draft, review); JA, EL, MN, SM, RP, RB, DS, SM, DPR, EMG, KB, TFL, AO, LN – methodology, investigation, formal analysis; KV, ELV, MA, NS – methodology, investigation, formal analysis, software; RP – conceptualization, methodology, investigation, formal analysis; PJLR, JS, AP – resources; ZG, BT, AM, JM, AC, VQ – conceptualization, funding acquisition, writing (review); EC – supervision, conceptualization, project administration, funding acquisition; writing (review and editing); TA – supervision, conceptualization, methodology, investigation, formal analysis, funding acquisition, project administration, writing (original draft, review and editing) (https://www.casrai.org/credit.html).

SUPPLEMENTAL REFERENCES

Avril T, Vauleon E, Hamlat A, et al. Human glioblastoma stem-like cells are more sensitive to allogeneic NK and T cell-mediated killing compared with serum-cultured glioblastoma cells. *Brain pathology*. 2012;22(2):159-174. doi:10.1111/j.1750-3639.2011.00515.x

Bowman RL, Klemm F, Akkari L, et al. Macrophage Ontogeny Underlies Differences in Tumor-Specific Education in Brain Malignancies. *Cell Rep*. 2016;17(9):2445-2459. doi:10.1016/j.celrep.2016.10.052

Chevet E, Doultsinos D, Eriksson L a, et al. Compounds Containing a Hydroxyphenyl Moiety and Their Use. 2023;(EP22305014A·2022-01-07).

Cui X, Wang Q, Zhou J, et al. Single-Cell Transcriptomics of Glioblastoma Reveals a Unique Tumor Microenvironment and Potential Immunotherapeutic Target Against Tumor-Associated Macrophage. *Front Oncol*. 2021;11:710695. doi:10.3389/fonc.2021.710695

Hussain, et al., 2006

Le Reste PJ, Pineau R, Voutetakis K, et al. Local intracerebral inhibition of IRE1 by MKC8866 sensitizes glioblastoma to irradiation/chemotherapy in vivo. *Cancer Lett*. 2020;494:73-83. doi:10.1016/j.canlet.2020.08.028

Lhomond S, Avril T, Dejeans N, et al. Dual IRE1 RNase functions dictate glioblastoma development. *EMBO molecular medicine*. Published online January 8, 2018. doi:10.15252/emmm.201707929

Parney IF, Waldron JS, Parsa AT. Flow cytometry and in vitro analysis of human glioma–associated macrophages. *J Neurosurg.* 2009. 110(3): 572–582. https://doi.org/10.3171/2008.7.JNS08475

Yin W, Ping YF, Li F, et al. A map of the spatial distribution and tumour-associated macrophage states in glioblastoma and grade-4 IDH-mutant astrocytoma. *J Pathol*. Published online June 20, 2022. doi:10.1002/path.5984

SUPPLEMENTAL TABLES

Table S1. Antibodies used in the study

Targets	Species	Compagny
Human		
Actin	mouse monoclonal	Sigma Aldrich
KDEL	mouse monoclonal	Enzo
IκB	rabbit polyclonal	Cell Signaling
phospho-IκB	rabbit monoclonal	Cell Signaling
IRE1	rabbit polyclonal	Santa Cruz
UBE2D3	mouse monoclonal	Abcam
NFκB p65	rabbit monoclonal	Cell Signaling
phospho-NFκB p65	rabbit monoclonal	Cell Signaling
Tubulin	mouse monoclonal	Sigma Aldrich
XBP1s	mouse monoclonal	BioLegend
VCP	mouse monoclonal	BD Transduction Laboratories

Table S2. Primers used in the study

Gene	Forward primer	Reverse primer
Human		
ACT	5'-CATGGGTGGAATCATAATGG-3'	5-AGCACTGTGTTGCGCTACAG-3
CCL2	5'-AGAATCACCAGCAGCAAGTGTCC-3'	5'-TCCTGAACCCACTTCTGCTTGG-3'
CXCL2	5'-CTGCGCTGCCAGTGCTT-3'	5'-CCTTCACACTTTGGATGTTCTTGA-3'
GAPDH	5'-AAGGTGAAGGTCGGAGTCAA-3'	5'-CATGGGTGGAATCATAATGG-3'
IL6	5'-GGTACATCCTCGACGGCATCT-3'	5'-GTGCCTCTTTGCTGCTTTCAC-3'
IL8	5'-TGGCAGCCTTCCTGATTTCT-3'	5'-GGGTGGAAAGGTTTGGAGTATG-3'
MIB1	5′-ACTGGCAGTGGGAAGATCAA-3′	5′-CATATGCTGCGCTATGTGGG-3′
IRE1	5'-GCCACCCTGCAAGAGTATGT-3'	5'-ATGTTGAGGGAGTGGAGGTG-3'
UBE2D3	5'-CCGGACCTTTGAGCATACAC-3'	5'-GCCTTGATATGGGCTGTCAT-3'
XBP1tot	5'-CCTGGTTCTCAACTACAAGGC-3'	5'-AGTAGCAGCTCAGACTGCCA-3'
XBP1s	5'-TGCTGAGTCCGCAGCAGGTG-3'	5'-GCTGGCAGGCTCTGGGGAAG-3'
Mouse		
actb	5'-CATTGCTGACAGGATGCAGAAGG-3'	5'-TGCTGGAAGGTGGACAGTGAGG-3'
ccl2	5'-GCTACAAGAGGATCACCAGCAG-3'	5'-GTCTGGACCCATTCCTTCTTGG-3'
cxcl2	5'-CATCCAGAGCTTGAGTGTGACG-3'	5'-GGCTTCAGGGTCAAGGCAAACT-3'
gapdh	5'-CATCACTGCCACCCAGAAGACTG-3'	5'-ATGCCAGTGAGCTTCCCGTTCAG-3'
g-csf	5'-ATCCCGAAGGCTTCCCTGAGTG-3'	5'-AGGAGACCTTGGTAGAGGCAGA-3'
il1b	5'-TGGACCTTCCAGGATGAGGACA-3'	5'-GTTCATCTCGGAGCCTGTAGTG-3'
il6	5'-TACCACTTCACAAGTCGGAGGC-3'	5'-CTGCAAGTGCATCATCGTTGTTC-3'
lif	5'-TCAACTGGCACAGCTCAATGGC-3'	5'-GGAAGTCTGTCATGTTAGGCGC-3'

Table S3. Probes designed for the gel shift assays

Site	Probe sequence
Human	
h1	5' BIOT – tctaattaacccttactctcaagttattATAATAACGTGGCCTCAaaaattcatgtaataagaccctggcacaccac - 3'
h2	5' BIOT - tggtcacttgaacagtatacattagactacttatattcatcaTTGTTGACGTGTTAAGTttttattaggtaaaactttctgcaacagtt - 3'
h3	5' BIOT – aaggtgctgttccgagaagaaggaaaaggGCTTGACACGTATTCACtcggccccggacgtgggaagcaagccgtctggcttcggcctac - 3'
h4	5' BIOT - ccgaaagcacggtacagaggctgttggtggCTTTGCCACGCCACCCCcccaccccggatcgcggctgtcttaagggacc - 3'
Mouse	
m1	5' BIOT – tgcctgcaacaggttctcaaaattcaaattatttccaCGTAGTCCTGAAGGACCTCCACTTTaagtagggtcgtttaaggatgctaga- 3'
m2	5' BIOT - cctcagttcgctaaaatgtggtgacGAAGTCTGTTCAGAAGCTTAACCaaatctgggcagttacacaagag- 3'

SUPPLEMENTAL FIGURE LEGENDS

Figure S1. Impact of IRE1 on myeloid recruitment to GB *in vitro* and *in vivo*.

(A) Barcode plot representation of the enrichment of immune cell gene signatures characterizing polynuclear neutrophils (PMN), microglia/macrophages (MM) and T cells observed in GB specimens (TCGA cohort) based on high (n=264) or low (n=275) IRE1 activity obtained from (Lhomond *et al.* 2018). **(B)** mRNA expression of specific markers CD14, CD15 and CD4 corresponding to immune PMN, MM and T cells in GB specimens from the TCGA cohort categorized according to their IRE1 high (n=264) or low (n=275) activity. *p* value obtained from unpaired t-test comparing IRE1 high versus low tumors. **(C)** Total immune infiltrates of human GB tissues (n=65) were analyzed on living cells (7AAD negative) by flow cytometry using anti-CD45 and anti-CD11b antibodies. An example of flow cytometry analysis with the GB specimen GBM#175 is presented. **(D)** MM populations co-expressed monocytic markers such as CD14, CD163 and CD64, but did not express CD66B and CD3. An example of flow cytometry analysis with the GB specimen GBM#139 is presented. **(E)** PMN and T populations expressed CD66b and CD3 respectively but not the MM marker CD14. An example of flow cytometry analysis with two GB specimens GBM#129 and #164 is presented. **(F)** Characterization of the different subtypes of immune cells was performed combining the CD45 marker with specific markers i.e. MM markers CD11c, CD33, CD105, HLA-DR, as well as CD14, CD64 (specific for MDM/MMG) and CD163 (specific for MDM); PMN markers CD15, CD16 and CD66b; and T cell markers CD3 and CD8. **(G)** Characterization of neutrophils isolated from blood using flow cytometry based on the expression of specific markers as designated. **(H)** Immunoblot analysis of the expression of wild-type (WT) (upper band - 110 kDa) or Q780* IRE1 (truncated form, lower band - 80 kDa), as well as that of XBP1s in RADH87 primary cell line exposed to tunicamycin treatment (Tm, 5 µg/mL for 6h). Actin (ACT) was used as loading control. **(I)** Quantification of IRE1 WT, IRE1 Q780* and XBP1s protein expression from the Western blot analysis (n=4 biological replicates, mean ± SD). *p* values according to an ANOVA test comparing parental, IRE1 WT or Q* cells. **(J)** Basal XBP1s mRNA expression observed in parental RADH87 and IRE1 WT and Q780* over-expressing RADH87 cell lines (n=3 biological replicates, mean ± SD). *p* values according to an ANOVA test comparing parental, IRE1 WT or Q* cells. **(K)** mRNA expression of CCL3, CCL5, CCL8 (chemokines for MM) and CXCL1, CXCL5 and CXCL7 (chemokines for PMN) in the population of tumors with high (red) or low (blue) MM and PMN infiltration, as determined according to CD14 or CD15 levels respectively. CD14 and CD15 high and low groups were determined using the median of the marker mRNA expression as cut-off (high/low n=263/263). *p* values according to unpaired t-test comparing CD14 and CD15 high versus low tumors.

Figure S2. IRE1-dependent regulation of UBE2D3 expression in GB cells and its impact of NFκB signaling.

(A) Western blot analysis of NFκB expression as well as NFκB phosphorylation in parental U87 and U87 DN cells. HSP90 was used as control of protein loading. Quantification of total and phospho-NFκB expression from the Western blot analysis (n=3 biological replicates, mean). *p* values according to unpaired t-test comparing parental to DN U87 cells. **(B)** Quantification of XBP1s mRNA expression by RT-qPCR in U87 cells treated for 24 hours with the IRE1 activator IXA4, the IRE1 inhibitor MKC8866 (MKC) and DMSO alone (used as negative control) (n=5, 2 and 3 biological replicates respectively, mean). *p* value according to an ANOVA test comparing the three conditions. **(C)** Western blot analysis of UBE2D3 in parental (-) and U87 cells treated for 24 hours with MKC8866 (MKC), IXA4 and DMSO (control). Actin (ACT) was used as loading control. Three biological replicates are presented. **(D)** Western blot analysis of IRE1 and UBE2D3 in U87 cells silenced for IRE1 using a siRNA approach. Actin (ACT) was used as loading control. Three replicates from three independent experiments are presented. **(E)** Quantification of XBP1s mRNA expression by RT-qPCR in U87 and RADH87 cells silenced or not (siCTR) for XBP1 (siXBP1) during 48 hours (n=3 biological replicates, mean). *p* value according to an ANOVA test comparing the three conditions. **(F)** Western blot analysis of UBE2D3 in U87 and RADH87 cells silenced for XBP1 using a siRNA approach during 48 hours. Actin (ACT) was used as loading control. Three biological replicates are presented. The framed parts were used in Figure 3G. **(G)** Western blot analysis of UBE2D3 in RADH87 cells silenced for XBP1 using a siRNA approach during 96 hours. **(H)** Graphical representation of putative XBP1s binding sites (delineated in green) on the mouse ube2d3 promoter regions as analyzed with MatInspector and TFBIND. **(I)** Gel shift assays performed on 2 putative XBP1s binding sites using mouse GL261 nuclear extracts after tunicamycin treatment. Validation of putative binding sites *m1* in mouse using gradual amount (10, 20 and 200 fold) of unlabeled probes used in competition assay. **(J)** mRNA expression of SYVN1 in GB specimens from the local GBMmark cohort described in (Avril et al. 2017) and categorized according to their IRE1, XBP1s and RIDD activity (IRE1 high n=55 and low n=64; XBP1s high n=44 and low n=75; and RIDD high n=64 and low n=55) as described in (Lhomond et al., 2018). *p* values obtained from unpaired t-test comparing IRE1, XBP1s and RIDD high versus low tumors. **(K)** Association of NFκB signaling gene signature with SYVN1 low and high GB specimens from the local GBMmark cohort described in (Avril et al. 2017) (Lhomond et al., 2018). SYVN1 high and low groups were determined using the median of the marker mRNA expression as cut-off (high/low n=59/59).

Figure S3. Impact of XBP1s and RIDD branches on myeloid recruitment to GB in human specimens.

(A) TCGA GB patients clustering based on high/low XBP1 and RIDD activities were confronted to immune markers for MM, MDM, MG, PMN and T cells. UP (n) and *p* values denote the proportion of signature genes that were found up-regulated between the groups (n=number of genes) and the estimated two-sided directional *p*-value of test, respectively. **(B)** IRE1 high / XBP1s high or IRE1 high / RIDD high TCGA GB patients clustering based on high/low RIDD or XBP1s activity respectively were confronted to myeloid cell signatures. *p* values were obtained as described in (A).

Figure S4. Modulation of UBE2D3 expression and its impact of NFκB signaling.

(A-B) U87 and RADH87 cells were respectively transfected transiently or stably with empty vector (EV) or pCMV3-UBE2D3-Flag expression plasmid. Quantitative UBE2D3 mRNA expression was performed by RT-qPCR (n=3 biological replicates, mean ± SD) (A); and the level of UBE2D3 protein was observed with anti-UBE2D3 and anti-FLAG antibodies by Western-blot (n=2 and 3 biological replicates, mean ± SD) **(**B). *p* values according to unpaired t-test comparing parental or EV to UBE2D3 expressing cells. **(C)** Western blot analysis of NFκB, phospho-NFκB, IκB and phospho-IκB in RADH87 control (empty-vector, EV) cells and cells with transient UBE2D3. Actin (ACT) was used as loading control. **(D)** Quantification of NFκB and IκB expression as well as phospho-NFκB and phospho-IκB expression from the data presented in **Fig.5A** obtained in U87 and RADH87 control (empty-vector, EV) cells and in UBE2D3 overexpressing U87 (transient) and RADH87 (stable) cells (n=4 and 3 biological replicates respectively, mean). Actin (ACT) was used as loading control. *p* values according to unpaired t-test comparing EV to UBE2D3 over-expressing cells.

Figure S5. Impact of UBE2D3 on global proteins ubiquitination and its link to proteostasis.

(A) Schematic representation of the MS/MS experimental setup for the purification of ubiquitinated proteins from RADH87 control (EV) and UBE2D3 overexpressing cells. **(B)** Percentage of up- and downregulated proteins related to ER proteostasis or inflammation/immune response in RADH87_UBE2D3 cells compared to RADH87 control. **(C-D)** Representation of the ER-related protein network as identified in proteomics and list of statistically enriched GO biological processes (C) and GO cellular components (D). Indicated in colors are proteins, whose expression is modulated in UBE2D3 overexpressing cells (upregulated in red, downregulated in blue). **(E)** Volcano plots of differentially ubiquitinated proteins purified from control (EV) or UBE2D3 overexpressing RADH87 cells exposed or not to ER stressor, tunicamycin (Tun). Proteins with $p<0.05$ and log ratio >2 or log ratio <-2 are

delignated in pink and green, respectively. Dots represent purified peptides corresponding to the identified proteins. **(F)** List of ubiquitinated proteins significantly upregulated (pink) or downregulated (green) in the indicated conditions. EV, control RADH87 cells; UBETun, RADH87_UBE2D3 cells treated with tunicamycin. **(G)** Venn diagram corresponding to the ubiquitinated proteins upregulated or downregulated in the indicated conditions. **(H)** Overrepresented (pink) and underrepresented (green) GO biological processes for the set of purified ubiquitinated proteins from RADH87_UBE2D3 cells exposed to tunicamycin (Tun) compared to RADH87 control (EV) cells. Fold enrichment values are represented as the minus base 10 log of their corresponding *p* values. GO-term enrichments analysis was performed using STRING database.

Figure S6. UBE2D3 with MIB1 impacts on NFκB signaling and cytokines/chemokines production.

(A) Quantification of UBE2D3 mRNA level was performed by RT-qPCR on U87 cells over-expressing UBE2D3 and silenced or not (siCTR) for MIB1 (siMIB1) (n=2 biological replicates, mean). *p* values according to an ANOVA test comparing all conditions. **(B)** Quantification of NFκB, phospho-NFκB, IκB, and phospho-IκB proteins in transiently UBE2D3 overexpressing U87 cells after MIB1 down-regulation with a siRNA approach from the data presented in **Fig.6B**. siGL2 was used as silencing control (siCTR) (n=2 biological replicates, mean). Actin (ACT) was used as loading control. *p* values according to an ANOVA test comparing all conditions. **(C)** Quantification of MIB1 and UBE2D3 mRNA expression was performed by RT-qPCR on control (empty vector, EV) or UBE2D3 over-expressing RADH87 cells silenced or not (siGL2) for MIB1 (siMIB1) (n=3 biological replicates, mean ± SD). siGL2 was used as silencing control. (**): $p<0.01$, (***): $p<0.001$, (****): $p<0.0001$ according to unpaired t-test comparing control siGL2 to siMIB1 cells. **(D)** Quantification of CCL2, IL6, IL8 and CXCL2 mRNA expression using RT-qPCR in RADH87 cells overexpressing UBE2D3 and silenced or not for MIB1 (n=3 biological replicates, mean ± SD). siGL2 was used as silencing control. (*): $p<0.05$, (**): $p<0.01$, (***): $p<0.001$, (****): $p<0.0001$ according to unpaired t-test comparing control siGL2 to siMIB1 cells. **(E-H)** Migration of myeloid cells (Mo and PMN) isolated from blood of healthy donors in Boyden chamber assay towards media conditioned by UBE2D3 over-expressing RADH87 cells in the presence of anti-IL6 or -IL8 blocking antibodies (E); by parental (par.), control (siGL2) or UBE2D3 silenced U87 and RADH87 cells (F); by UBE2D3 silenced U87 or RADH87 cells in the presence of exogenous IL6 or IL8 cytokines (G); and by UBE2D3 over-expressing RADH87 cells silenced for MIB1 in the presence or not (PBS) of exogenous IL6 or IL8 cytokines (H) (n=3 biological replicates, mean ± SD). ns: not significant,

(*): $p<0.05$ (**): $p<0.01$, (***): $p<0.001$ according to unpaired t-test comparing to par., siGL2, PBS and CTR cells.

Figure S7. Effect of UBE2D3 overexpression on GB aggressiveness.

(A) Proliferative rate of GL261 parental and UBE2D3 overexpressing cells as determined using WST1-based colorimetric assay. The proliferation index was quantified by calculating the difference between the absorbance at 450 nm and that at 595 nm. **(B)** Quantification of *ccl2*, *cxcl2*, *il6*, *g-csf*, *il1b* and *lif* chemokines/cytokines mRNA expression levels using RT-qPCR in parental and UBE2D3 overexpressing GL261 cells (n=3 biological replicates, mean). *p* values according to unpaired t-test comparing parental to UBE2D3 expressing cells. **(C)** Migration of myeloid cells (Mo and PMN) isolated from blood of healthy donors in Boyden chamber assay towards fresh medium (-), media conditioned by parental (par.) and UBE2D3 overexpressing GL261 cells (n=3 biological replicates, mean ± SD). *p* values according to an ANOVA test comparing all conditions. **(D)** Proliferative rate of GL261 parental, control (sh CTR, two clones #1 & #2) and ube2d3 silenced (sh ube2d3, two clones #1 & #2) cells as determined using WST1-based colorimetric assay. The proliferation index was quantified by calculating the difference between the absorbance at 450 nm and that at 595 nm. **(E)** Quantification of *ccl2*, *cxcl2*, *il6*, *g-csf*, *il1b* and *lif* chemokines/cytokines mRNA expression levels using RT-qPCR in parental, control (sh CTR, two clones #1 & #2) and ube2d3 silenced (sh ube2d3, two clones #1 & #2) GL261 cells (n=3 biological replicates per clone, mean). *p* values according to unpaired t-test comparing parental to ube2d3 down-regulated GL261 cells. **(F)** Migration of myeloid cells (Mo and PMN) isolated from blood of healthy donors in Boyden chamber assay towards fresh medium (-), media conditioned by parental (par.), sh CTR and sh ube2d3 GL261 cells (n=3 biological replicates per clones, mean ± SD). *p* values according to an ANOVA test comparing all conditions. **(G-H)** Correlation between UBE2D3 mRNA level and indicated cytokines/chemokines expression in human GB cohort (G) and TCGA_GBLGG cohort (H). GFAP expression (astrocyte marker) was used as negative control. R square and *p* values of the slopes were calculated according to linear regression analyses between chemokines and UBE2D3 mRNA expression. **(I-J)** Correlation between UBE2D3 mRNA level and indicated immune cell-specific receptors expression in human GB cohort (I) and TCGA_GBLGG cohort (J). GFAP expression (astrocyte marker) was used as negative control. R square and *p* values of the slopes were calculated according to linear regression analyses between immune cell-specific receptors and UBE2D3 mRNA expression.

Figure S1

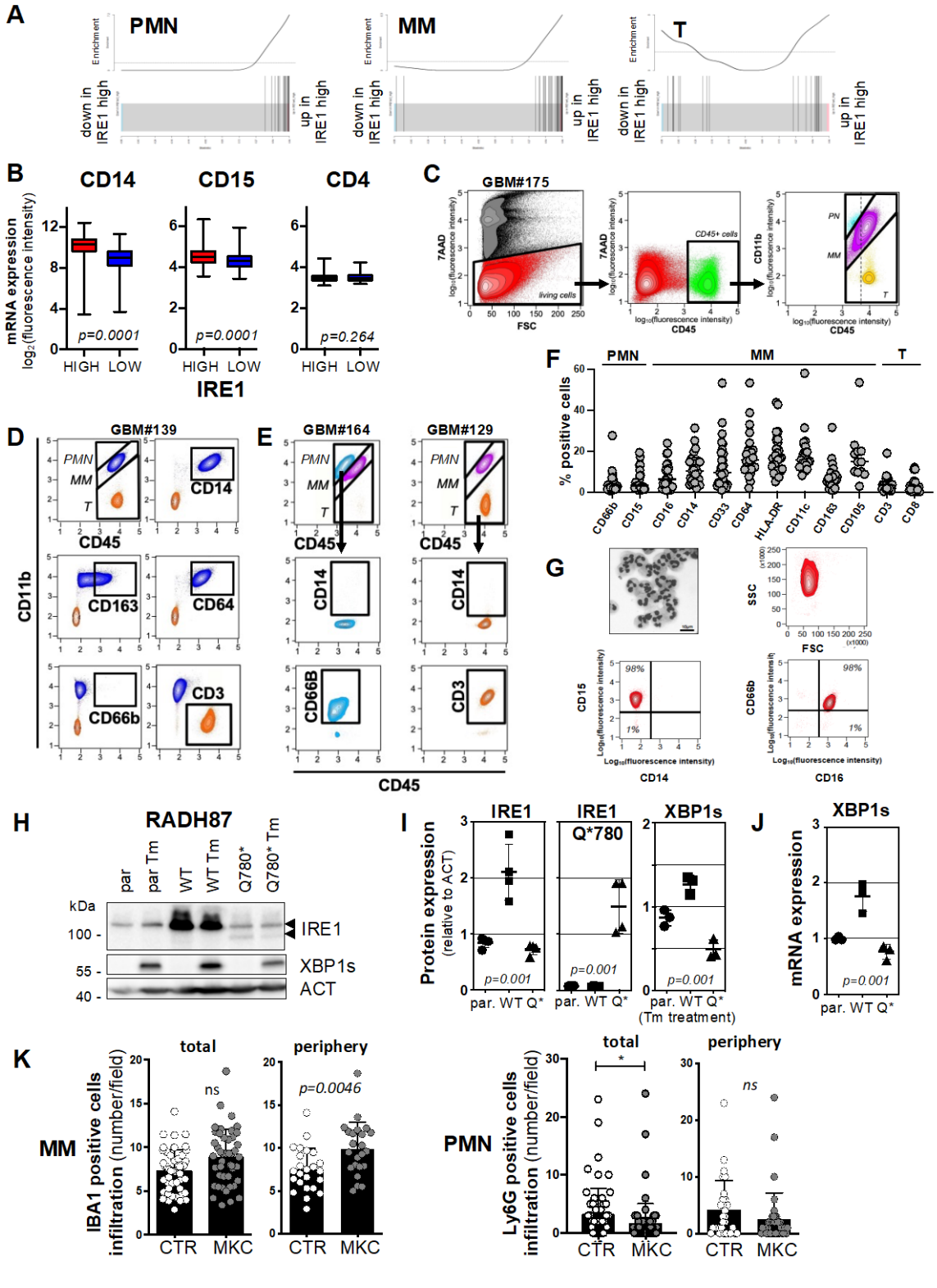

Figure S2

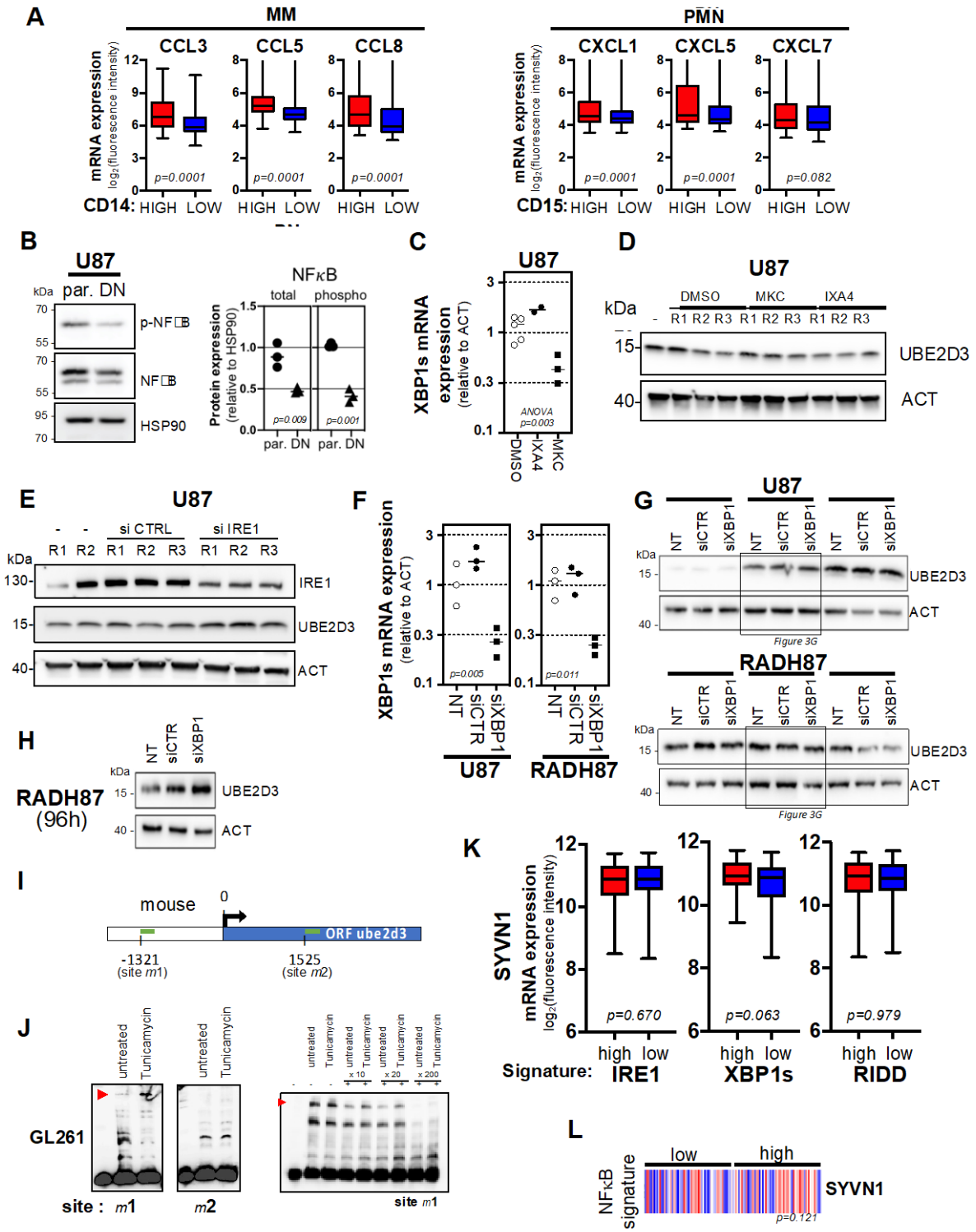

Figure S3

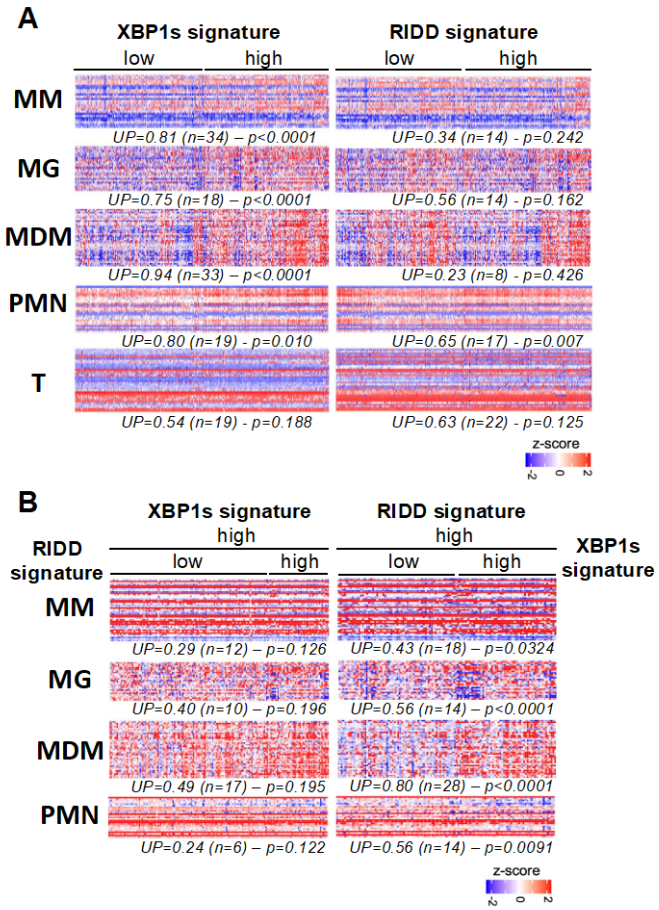

Figure S4

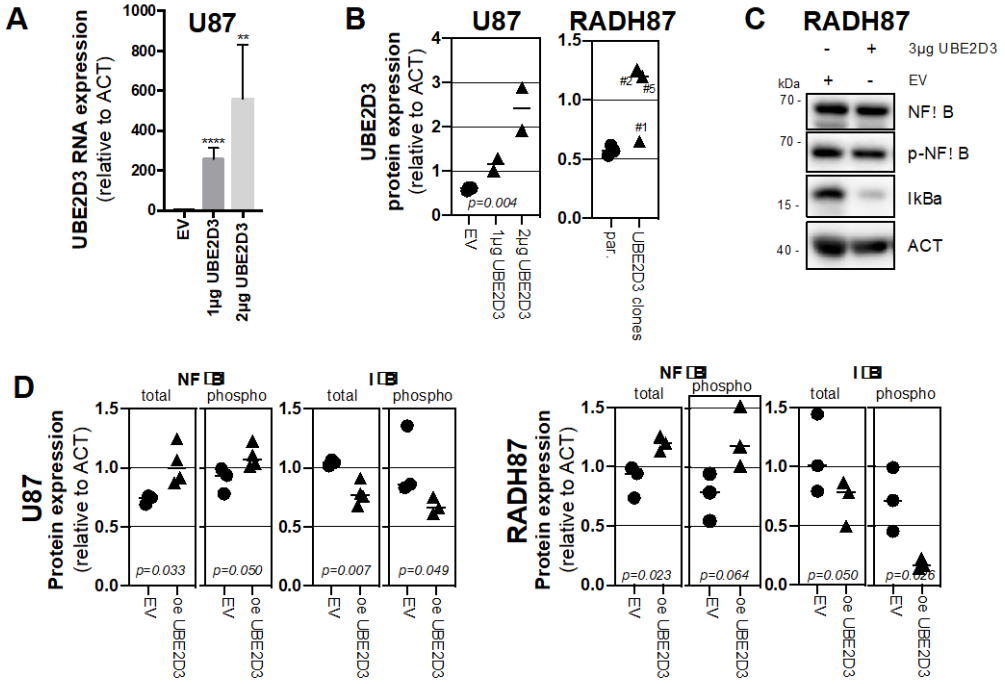

Figure S5

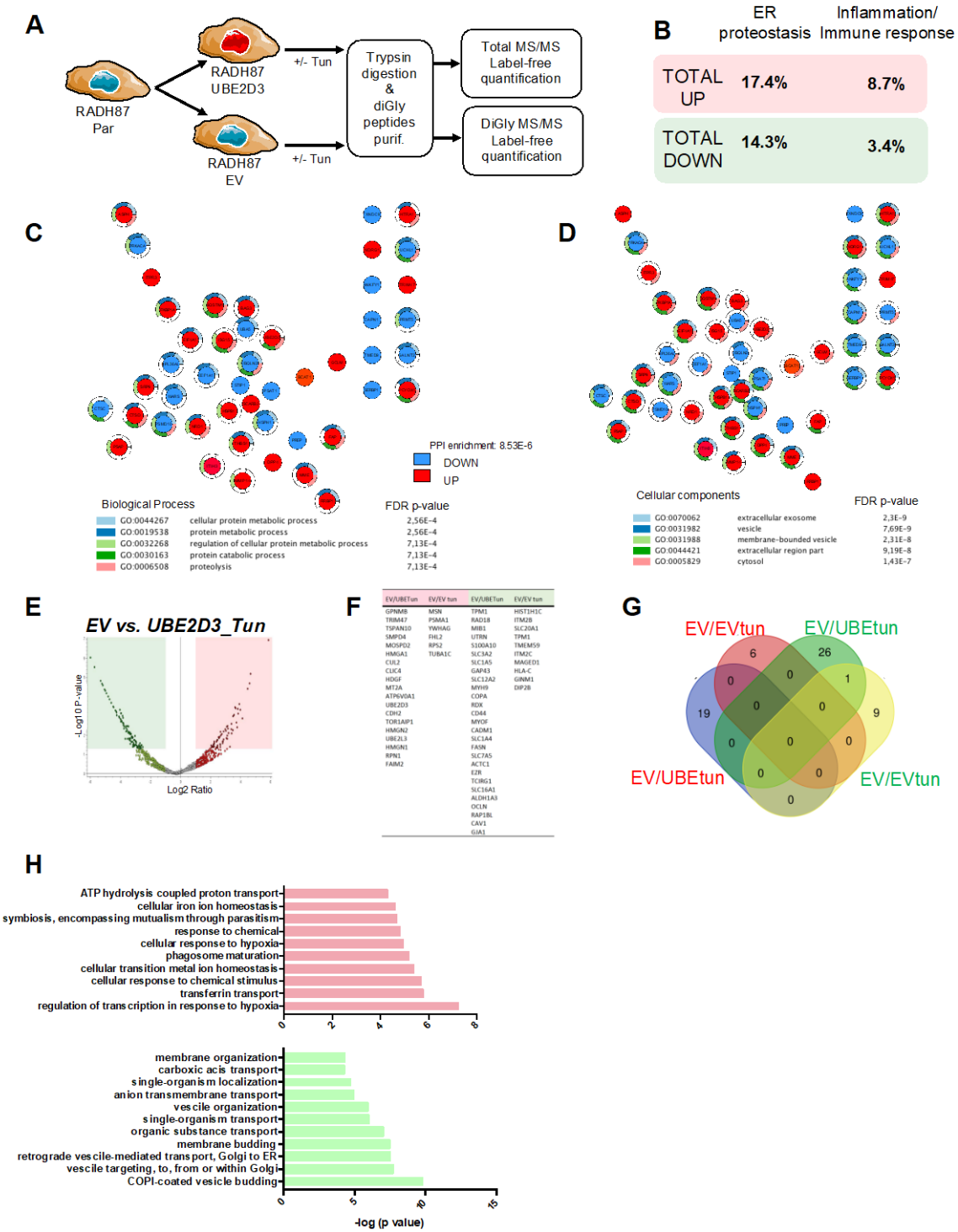

–

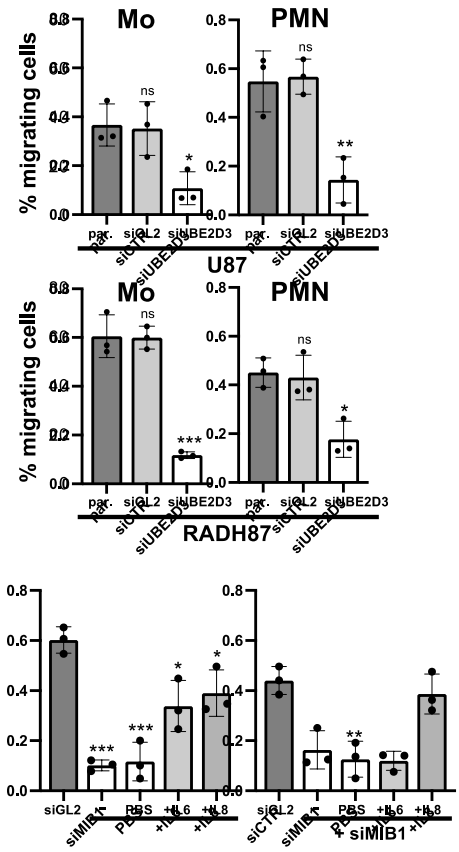

Figure S7